Computational Materials Science 227 (2023) 112287

Contents lists available at ScienceDirect

Computational Materials Science

journal homepage: www.elsevier.com/locate/commatsci

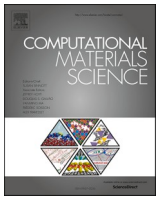

Full Length Article

An ab initio molecular dynamics study on $Ti_2AlN(0001)$ surfaces

Biao Yu [a], Yanfeng Han [a,*], Dong Li [a], Guangmin Hu [a], Qing Dong [a], Jiao Zhang [a,b], Baode Sun [a,b]

[a] Shanghai Key Lab of Advanced High-Temperature Materials and Precision Forming, School of Materials Science and Engineering, Shanghai Jiao Tong University, No. 800 Dongchuan Road, Shanghai 200240, China

[b] State Key Lab of Metal Matrix Composites, Shanghai Jiao Tong University, No. 800 Dongchuan Road, Shanghai 200240, China

ARTICLE INFO

Keywords:
Ti_2AlN surface
Ab initio molecular dynamics simulation
Surface energy
Electronic structure

ABSTRACT

The structures, surface energies, electronic properties of $Ti_2AlN(0001)$ surfaces at 0 K-1273 K were systematically investigated by ab initio molecular dynamics and first-principles calculations. It is found that the structural relaxations of Ti(N)- and Ti(Al)-terminated surfaces at all temperatures are mainly confined between outermost two layers, and those of N(Ti)- and Al(Ti)-terminated surfaces with Ti atoms at second layer extends into third layer. N(Ti)-terminated surface experiences the largest relaxation, and Al(Ti)-terminated surface possesses the least relaxation and is the most stable surface at all temperatures. The structural shrinkage relaxation of outermost two layers and surface energy for N(Ti)- and Ti(N)- terminated surfaces keep relatively stable from 0 K to 933 K, whereas dramatically increase from 933 K to 1273 K. The relaxation of outermost two layers for Al(Ti)- and Ti(Al)-terminated surfaces changes owing to the thermal expansion of the *d*-spacing of Al-Ti layers. The larger thermal expansion coefficient of the *d*-spacing of Al-Ti layers and faster surface energy decline of Ti(Al)-terminated surface than those of Al(Ti)-terminated surface indicate stronger metallic properties. The influence of redistribution of Ti-3d, N-2p and Al-3p orbitals on the electronic properties and structural relaxations of different termination surfaces at all temperatures range is elucidated.

1. Introduction

Ti_2AlN is one of MAX phases, which have a layered ternary hexagonal-structure (space group $P6_3/mmc$) with the general formula $M_{n+1}AX_n$ (where n = 1–3, M is transition metal, A is an IIIA or IVA subgroup element, and X is carbon or nitrogen). Like other MAX phases, Ti_2AlN with the combinations of strong Ti-N covalent-ionic bonding and relatively weak Ti-Al metallic bonding possesses both ceramic properties (low density, elastically stiffness, oxidation and corrosion resistance) and metallic properties (machinability, electrical and thermal conductivity, high hardness, damage and irradiation tolerance) [1–5]. The fascinating combination of these properties makes Ti_2AlN phase a potential candidate for load-bearing material at high temperatures [6,7], protective coating material against oxidation and corrosive environment [8,9], reinforcing and toughening particles in metal matrix composites (MMCs) [10–12].

Due to the excellent properties and wide applications of Ti_2AlN, significant attentions have been attracted from the theoretical viewpoint. A large number of theoretical data including crystal and electronic structures, mechanical properties, radiation tolerance, and thermodynamical properties of bulk Ti_2AlN phase were reported by density functional theory (DFT) calculations [1,13–16]. As mentioned above, Ti_2AlN is widely applied as coatings, thin film [17,18], reinforcing and toughening phases in MMCs. In these applications, the surface of Ti_2AlN rather than its bulk structure plays a more important role. For example, $Ti_2AlN(0001)$ surface can match with TiAl(1 1 1) surface as a coherent interface [19–21], and MAX phase thin films grow along the [0001] direction [17,18,22]. Owing to its crystal structure, the surface of Ti_2AlN is naturally (0001) basal planes terminated with single Ti, Al or N elements. A lot of MAX(0001) surfaces have been reported by DFT calculations [23–25]. Qureshi et al. [23] employed DFT to investigate the surface stability, electronic, and optical properties of (0001) surfaces of M_2AC (M = Zr, Hf, Cr; A = Al, Ga) at the ground state. Their calculations showed the charge density of valance Al-p and Ga-p electrons redistribute in the surface area, which is distinct from that for bulk structures. The A- and M(C)-terminated (0001) surfaces are the most stable and energetically favorable terminations. Liu et al.[13] investigated the structures, energies, electronic and defective properties of (0001), (10_10), (11_20) and (10_13) surfaces of Ti_2AlN at ground state using DFT. Their results showed that the Ti(Al)-, Al-terminated (0001)

* Corresponding author.
E-mail address: yfhan@sjtu.edu.cn (Y. Han).

https://doi.org/10.1016/j.commatsci.2023.112287
Received 28 February 2023; Received in revised form 23 April 2023; Accepted 23 May 2023
Available online 29 May 2023

surfaces experience the least relaxation and N-terminated (0001) surface experiences the greatest relaxation. The (0001)-TiAl, (0001)-Al surface are more stable under the condition of Ti- and Al-rich environments.

Based on Ti-Al metallic bonding and broad applications at high temperatures, temperature dependence on the surface structure of Ti_2AlN with different terminations cannot be neglected. Zhang et al.[3] found that temperature does play an important role in the nucleation and growth of Ti_2AlN thin films. Low temperature promotes growth of non-basal planes with low surface energies for Ti_2AlN, while high temperature facilitates basal plane growth on MgO (1 1 1) substrates. With 4.83% misfit between Ti_2AlN(0001) (a = 3.001 Å) and Al(1 1 1) (a = 2.856 Å) surfaces, Ti_2AlN may be both a potential nucleation substrate of Al atoms from liquid to solid during the solidification and potential reinforcing and toughening particles in Al matrix composites. The structural and thermodynamical stability of Ti_2AlN(0001) surface with different Ti, Al or N terminations above the melting temperature of Al to room temperature deicides the efficiency of heterogeneous nucleation of Al and the bonding mechanism of the interface between Ti_2AlN particles and Al matrix. It is a pity that there were few studies on the influence of temperature on Ti_2AlN surfaces up to now.

In this paper, systematic studies on the structures, energies and electronic properties of Ti_2AlN(0001) surfaces with different Ti, Al or N terminations were performed at different temperatures to understand their high temperature behaviors, and pave the way to further investigate the interface between Ti_2AlN and Al in the potential application of heterogenous nucleation during Al solidification and Ti_2AlN reinforced Al matrix composites.

2. Computational methods and models

All calculations were performed through Vienna ab initio simulation package (VASP) [26,27] using projector-augmented waves (PAWs) [28,29]. The exchange correlation functional was handled by the generalized gradient approximation (GGA) proposed by Perdew, Burke, and Ernzerh (PBE) [30]. A kinetic energy cut-off value of 400 eV was employed for plane wave expansions in reciprocal space. A self-consistent field (SCF) tolerance of 1×10^{-5} eV/atom was used for all SCF iterations. The valence electrons of N, Ti and Al atoms defined in the PAWs are $2s^2 2p^3$, $3p^6 3d^3 4s^1$, and $3s^2 3p^1$, respectively. The *k*-mesh was set as Gamma centered $3 \times 3 \times 1$, whereas a denser $15 \times 15 \times 1$ *k*-mesh was employed for the density of states (DOS) calculations. The static calculations were performed in the framework of DFT. The molecular dynamical simulations were calculated through ab initio molecular dynamics (AIMD). AIMD simulations were performed with canonical ensemble (NVT) and Nosé thermostat. To obtain the self-consistent charge density in the current study, we performed a static DFT calculation based on the optimized configuration by AIMD calculations.

Ti_2AlN is hexagonal layered structure with the space group $P6_3/mmc$ (1 9 4). Fig. 1(a) shows the atom occupations at the Wyckoff positions 2*a* [(0 0 0)] for N, 2*d* [(1/3 2/3 3/4)] for Al, and 4*f* [(1/3 2/3 0.085)] for Ti in unit cell. The highly symmetric hexagonal unit cell contains atomic layers of Ti, Al and N elements stacking along the c direction. Every two Ti layers sandwich one N layer to form a slab of Ti_2N composition stacking as a locally fcc-type sequence. A single Al atomic layer separates these slabs and forms mirror planes by following hcp stacking in the crystal. The calculated lattice parameters, *a* and *c*, of bulk Ti_2AlN presented in Table 1 were measured after full relaxation. Compared with the other reported experimental and theoretical data, our bulk calculation results show that the used parameters in this study are enough to ensure the calculation precision.

Owing to polar Ti_2AlN(0001) surfaces, we built symmetric surface slab models with Al layers as the middle layer, as seen in Fig. 1(b). In the supercell models, a vacuum slab of 15 Å thickness was employed at two sides to avoid long-range interactions of atoms at both ends. Supercell models were set as 3×3, as shown in Fig. 1(c), to ensure the precision of the relaxation at different temperatures. Four terminations of Ti_2AlN (0001) surface shown in Fig. 1(b) were considered by breaking Ti-Al and Ti-N bonds. Based on the atoms at outermost and second layer (in brackets), these surface models are named as N(Ti)-terminated, Ti(N)-terminated, Al(Ti)-terminated and Ti(Al)-terminated surfaces. To study the influence of layer thickness on surface properties, we constructed 12 supercells for these four models in total. The numbers of layers are 5, 13

Table 1
Calculated lattice parameters of Ti_2AlN.

Source	Lattice parameters (Å)	
	a	*c*
Present work	3.001	13.651
Experiment[31]	2.986	13.60
Experiment[32]	2.991	13.619
Theory[2]	3.01	13.70
Theory[33]	2.997	13.636
Theory[13]	2.998	13.608

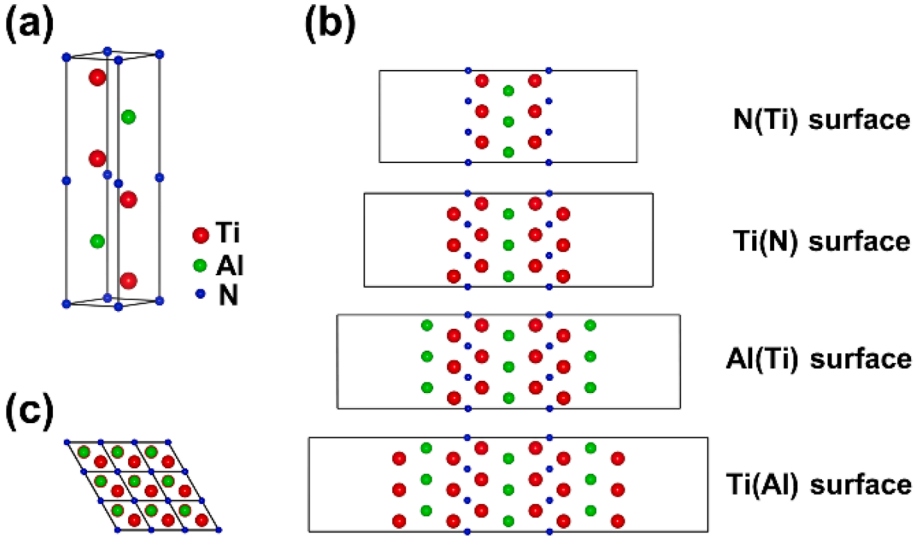

Fig. 1. (a) The hexagonal crystal structure of Ti_2AlN. (b)Four surfaces of Ti_2AlN(0001): N(Ti)-terminated surface, Ti(N)-terminated surface, Al(Ti)-terminated surface and Ti(Al)-terminated surface. (c) 3×3 supercell at top view. The red, green, and blue spheres represent Ti, Al and N atoms, respectively. (For interpretation of the references to colour in this figure legend, the reader is referred to the web version of this article.)

and 21 corresponding to N(Ti)-terminated surface. The supercells with 7, 15 and 23 layers, 9, 17 and 25 layers, 11, 19 and 27 layers are corresponding to Ti(N)-terminated, Al(Ti)-terminated and Ti(Al)-terminated surfaces, respectively.

3. Results and discussion

3.1. Influence of temperature on lattice parameters of bulk Ti_2AlN

As mentioned in the introduction, Ti_2AlN is a potential nucleation substrate of Al atoms from liquid to solid, and a strengthening phase for aluminum matrix composites. The temperature above the melting point of Al to room temperature should be considered in the calculations. Therefore, the temperatures set at 0 K, 273 K, 600 K, 933 K and 1273 K were considered around the melting point of aluminum, 933 K, for Ti_2AlN bulk and surface calculations. The calculated lattice parameters of bulk Ti_2AlN at these temperatures are shown in Fig. 2. It is seen that the lattice is linearly expanded with increasing temperature from 273 K to 1273 K. The average coefficients of thermal expansion (CTE) of Ti_2AlN along *a* and *c* axes from 273 K to 1273 K calculated by the slopes of fitted lines are listed in Table 2. Our calculated results coincide with the reported experimental values [5], which further confirms the accuracy of our simulation at heating states. Accordingly, the calculated lattice parameters of bulk Ti_2AlN are applied in the following AIMD simulations of $Ti_2AlN(0001)$ surfaces at the corresponding temperatures.

3.2. Relaxations of Ti_2AlN surfaces

The AIMD simulations of Ti_2AlN surface relaxations consist of two parts: full relaxation and precise measurement. In relaxation part, the 2 ps AIMD simulations with time step as 0.5 fs can ensure the final equilibrium and a convergence with the Hamiltonian fluctuation less than 0.1‰. In precise measurement part, the time step was employed as 0.2 fs for 0.4 ps AIMD simulations to improve the precision of measuring the *d*-spacing by reducing the movement step.

The *d*-spacings between neighboring layers for $Ti_2AlN(0001)$ surface along the normal direction were calculated using Z-directional atomic density ($\rho(z)$) profile, which can be calculated as:

$$\rho(z) = \frac{\langle N_z \rangle}{A_{xy}\Delta z} \tag{1}$$

where Δz means the interval length dividing the entire model at Z direction, $\langle N_z \rangle$ represents the number of atoms in the area of Z-direction $(z - \Delta z/2,\ z + \Delta z/2)$ of selected steps, A_{xy} denotes the surface area of

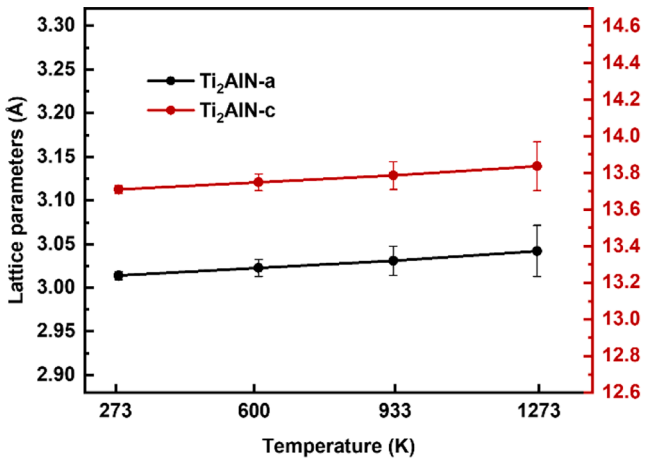

Fig. 2. The calculated lattice parameters of bulk Ti_2AlN at 273 K, 600 K, 933 K and 1273 K.

Table 2
Coefficient of thermal expansion (CTE) for Ti_2AlN.

Source	CTE (10^{-5}/°C)	
	a	c
Present work	1.2742	1.1569
Experiment [5]	1.2746	1.1493

four surface models along (0001) surface. Δz was set as 0.01 Å and the last 0.1 ps simulation with 500 steps of AIMD simulations was used to analyze $\rho(z)$. For example, Fig. 3 shows the $\rho(z)$ profiles of Al(Ti)-terminated (0001) surface with 17 layers at 1273 K after full relaxation.

After obtaining the *d*-spacings between neighboring layers, the relaxations of four surface models at different temperatures can be written as follows:

$$\Delta d_{ij} = \frac{d_{ij} - d_{ij,bulk}}{d_{ij,bulk}} \times 100\% \tag{2}$$

where d_{ij} represents the *d*-spacing between i^{th} and j^{th} layers after relaxation, and $d_{ij,bulk}$ denotes the *d*-spacing between the atoms of i^{th} and j^{th} layers in bulk structure. Two types of the *d*-spacings of neighboring layers exist in Ti_2AlN along [0001], d_{Ti-N} (the *d*-spacing between Ti and N neighboring layers) and d_{Ti-Al} (the *d*-spacing between Ti and Al neighboring layers).

After full relaxation, Δd_{Ti-Al} and Δd_{Ti-N} of the innermost Al, Ti and N layers of four surface models at five temperature points are drawn in Fig. 4. The results show that Δd_{Ti-Al} of innermost Al-Ti layers is sensitive to system temperature and linearly expands except that of the surface model with 5 atomic layers. Δd_{Ti-N} of second inner Ti layer and third inner N layer almost keeps steady with increasing temperature. It should be mentioned that the surface model with 5 atomic layers is not thick enough to represent N(Ti)-terminated surface with inner bulk structure, wherein the model only possesses d_{12} and d_{23} along N, Ti and Al atomic layers. To guarantee the inner bulk structure, the atomic layers of Ti_2AlN (0001) surface slab should be more than 7. The average CTEs of the inner Al, Ti and N layers calculated by the slopes of fitted lines in Fig. 4 are nearly $1.92 \pm 0.20 \times 10^{-5}$/K for d_{Ti-Al} and $-0.10 \pm 0.10 \times 10^{-5}$/K for d_{Ti-N}. Considering the above-calculated CTEs of d_{Ti-N} and d_{Ti-Al} and their initial parameters of bulk Ti_2AlN at 0 K as 1.16524 Å and 2.24756 Å, respectively, the CET of bulk Ti_2AlN can be calculated as follows:

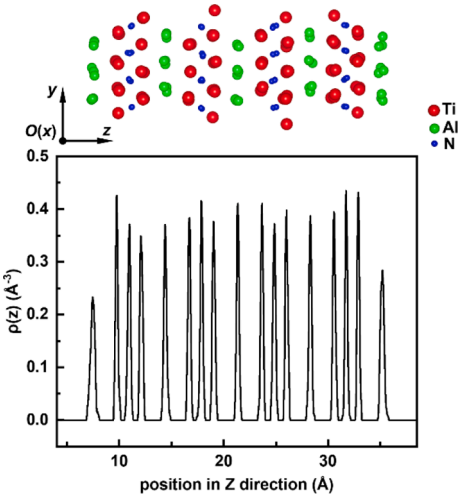

Fig. 3. Z density profiles of Al(Ti)-terminated surface with 17 atomic layers at 1273 K. The red, green, and blue spheres represent Ti, Al and N atoms, respectively. (For interpretation of the references to colour in this figure legend, the reader is referred to the web version of this article.)

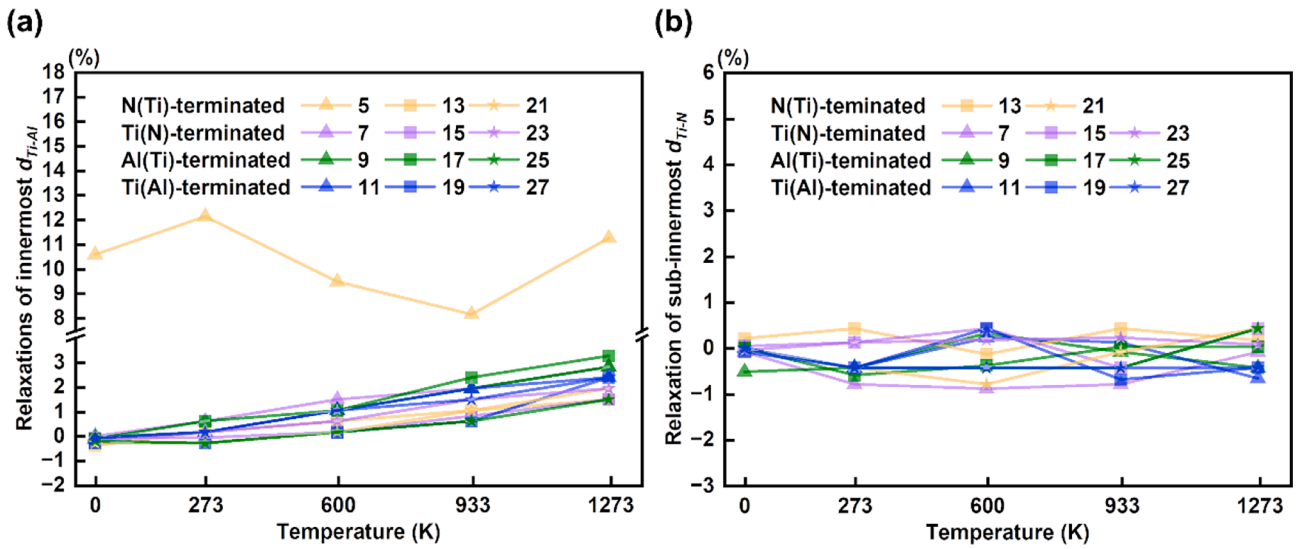

Fig. 4. Relaxations of two types of neighboring inner layers in Ti_2AlN(0001) surfaces at 0 K, 273 K, 600 K, 933 K and 1273 K. (a) Δd_{Ti-Al}; (b) Δd_{Ti-N}.

$$CTE_{Ti_2AlN} = CTE_{Ti-N}\frac{d_{Ti-N}}{d_{Ti-N}+d_{Ti-Al}} + CTE_{Ti-Al}\frac{d_{Ti-Al}}{d_{Ti-N}+d_{Ti-Al}} \quad (3)$$

The calculated CET of bulk Ti_2AlN is 1.23×10^{-5}/K, which is in accordance with the value along *c* axis by bulk calculation in section 3.1.

The temperature dependence of relaxations of the *d*-spacings near Ti_2AlN(0001) surface was measured and shown in Fig. 5. Compared with the inner Δd shown in Fig. 4, the similar curves of Δd_{34} were presented in Fig. 5(e) and (f). The average CTEs of d_{34} for d_{Ti-Al} and d_{Ti-N} are $1.94 \pm 0.16 \times 10^{-5}$/K and $-0.11 \pm 0.13 \times 10^{-5}$/∘C, indicating the structural relaxations of all surfaces are mainly confined among the outermost three layers.

Δd_{12} of these surfaces at ground state (0 K) shown in Fig. 5(a) and (b) are sorted as Al(Ti)-terminated (-1.01 ± 0.22%) > Ti(Al)-terminated (-1.67 ± 0.10%) > Ti(N)-terminated (-3.02 ± 0.10%) > N(Ti)-terminated (-37.35 ± 0.10%), which is in agreement with the early reports at the ground state [13]. Overall, N(Ti)-terminated surface shows the largest shrinkage relaxation. For Ti_2AlN(0001) surfaces with the outermost two layers composed of Ti and N atoms, structural relaxation between Ti and N layers for both N(Ti)- and Ti(N)-terminated surfaces keeps stable from 0 K to 933 K and dramatically increases from 933 K to 1273 K. The covalent Ti-N bondings are expected to be strengthened from 933 K to 1273 K. For Ti_2AlN(0001) surfaces with the outermost two layers composed of Ti and Al atoms, Δd_{12} are increased with temperature improved. The *d*-spacings of Ti and Al layer shrink below 600 K and then expand above 600 K compared with that of the inner layers. The average CTE of d_{12} of Al(Ti)-terminated surface is $2.21 \pm 0.15 \times 10^{-5}$/K from 0 K to 1273 K, which is a little bigger than that of inner d_{Ti-Al}, $1.94 \pm 0.16 \times 10^{-5}$/K. The average CTE of d_{12} of Ti(Al)- terminated surface from 0 K to 1273 K is $3.88 \pm 0.15 \times 10^{-5}$/K, much larger than that of Al(Ti)-terminated surface, indicating that the metallic property of Ti(Al)-terminated surface is stronger than that of Al(Ti)-terminated surface.

Δd_{23} of these surfaces were measured and presented in Fig. 5(c) and (d). Compared with inner Δd_{Ti-Al} and Δd_{Ti-N} in Fig. 4, it is worth noticing that the d_{23} of Ti(Al)- and Ti(N)-terminated surfaces show the bulk features. At 0 K, Δd_{23} of N(Ti)-terminated surface is 8.40 ± 0.05% and Δd_{23} of Al(Ti)-terminated surface is 1.40 ± 0.05%, which is much larger than that of inner Δd, indicating their surface features. For N(Ti)- and Ti(Al)-terminated surfaces, d_{23} of Ti and Al layers linearly expands from 0 K to 1273 K. Their average CTEs are $1.95 \pm 0.10 \times 10^{-5}$/K and $1.93 \pm 0.15 \times 10^{-5}$/K, respectively, which are close to the value of inner d_{Ti-Al}. For Ti(N)- and Al(Ti)-terminated surfaces, d_{23} of Ti and N layers is insensitive to temperature. The average CTEs are $-0.03 \pm 0.10 \times 10^{-5}$/∘C and $-0.15 \pm 0.06 \times 10^{-5}$/∘C, respectively, which are close to the value of inner d_{Ti-N}.

3.3. Surface energy

Surface energy plays a vital role in predicting the thermodynamic stability of surface configuration. In this study, the surface energy of 12-layered slabs with 7 single-sided layers fixed is calculated by subtracting the relaxation energy from the cleavage energy of two sets complementary of surfaces (Ti(N) and Al(Ti), and Ti(Al) and N(Ti)) sharing the same cleavage energy, which has been successfully used in the early reports [23,24], as follows:

$$\gamma = \frac{E_{unrelaxed} - NE_{bulk}}{2A} + \frac{E_{relaxed} - E_{unrelaxed}}{A} \quad (4)$$

where E_{bulk} is the calculated bulk energy of a single cell of Ti_2AlN with 8 atomic layers along [0001] direction, $E_{unrelaxed}$ is the static energy of the surface model after cleavage, $E_{relaxed}$ is the value after surface relaxation, *N* is 1.5 as the ratio of layers between the surface model and single cell, and *A* denotes the surface area varying with temperature. The parameters of AIMD simulations were set the same as those in the above surface relaxations.

Fig. 6 shows the temperature dependence of surface energy of four types of Ti_2AlN(0001) surfaces from 0 K to 1273 K. At the ground state, the surface energies of Al(Ti)- and N(Ti)-terminated models are 2.602 J/m^2 and 2.824 J/m^2, respectively, while those of Ti(N)- and Ti(Al)-terminated models are 3.523 J/m^2 and 5.530 J/m^2. The surface energies for Al(Ti)- and Ti(Al)-terminated models are linearly decreased with increasing system temperature from 0 K to 1273 K. The descent speeds of surface energy for Al(Ti)- and Ti(Al)-terminated models are -0.947×10^{-3}J/(m^2·K) and -1.967×10^{-3}J/(m^2·K), respectively, corresponding to the larger expansion of d_{12} for Ti(Al)-terminated surface than Al(Ti)-terminated surface in Fig. 5(b). It is worth noticing that the surface energies of N(Ti)- and Ti(N)-terminated models almost keep stable below 933 K. While they rapidly increase from 933 K to 1273 K, which is consistent with the above dramatical decrease of d_{12} for these two surfaces in Fig. 5(a). The trend for the surface energy between 0 K and 933 K is in an order of Al(Ti)-terminated < N(Ti)-terminated < Ti(N)-terminated < Ti(Al)-terminated. The surface energies of N(Ti)- and Ti(N)-terminated models are larger than those of Al(Ti)- and Ti(Al)-terminated models with increasing system temperature as 1273 K. In the view of thermodynamic, Al(Ti)-terminated surface is the most stable at all the temperatures studied in our work. It can be predicted that the

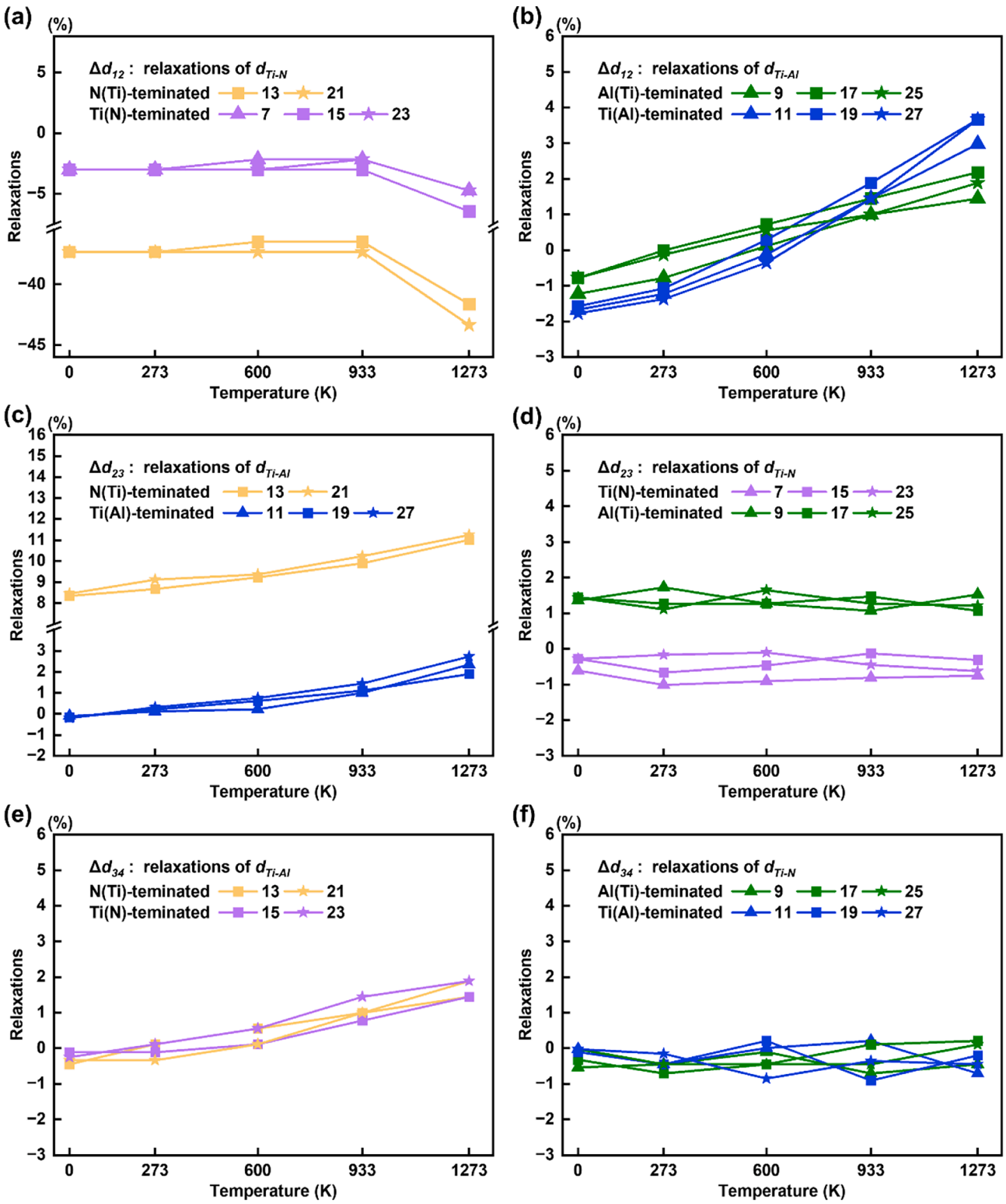

Fig. 5. Relaxations of the *d*-spacings near $Ti_2AlN(0001)$ surfaces at 0 K, 273 K, 600 K, 933 K and 1273 K. Δd_{12}: (a) Δd_{Ti-N} and (b) Δd_{Ti-Al}; Δd_{23}: (c) Δd_{Ti-Al} and (d) Δd_{Ti-N}; Δd_{34}: (e) Δd_{Ti-Al} and (f) Δd_{Ti-N}.

surface energies for Al(Ti)- and Ti(Al)-terminated are smaller than that of N(Ti)- and Ti(N)-terminated above 1273 K until 1673 K where Ti_2AlN is decomposed as TiN_x and aluminum steam [5]. The predicted surface energies of Al(Ti)- and Ti(Al)-terminated surfaces at 1673 K calculated by the slopes of fitted lines are 1.018 J/m^2 and 2.239 J/m^2, indicating that Al(Ti)-terminated surface is the most stable surface at all temperatures until its decomposition.

3.4. Surface electronic properties

Four types of $Ti_2AlN(0001)$ surface models, N(Ti)-terminated with 13 atomic layers, Ti(N)-terminated with 15 atomic layers, Al(Ti)-terminated with 17 atomic layers and Ti(Al)-terminated with 19 atomic layers, are chosen to investigate surface electronic properties. The calculated total DOS and layered PDOS of these surfaces at ground

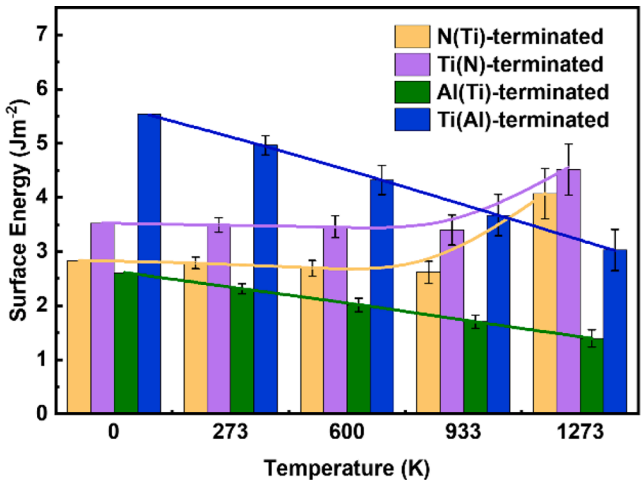

Fig. 6. Surface energy of four $Ti_2AlN(0001)$ surfaces at 0 K, 273 K, 600 K, 933 K and 1273 K.

state are shown in Fig. 7. The Fermi energy level denoted by a dashed line is set to zero. From the total DOS, the metallic property of all surface models is confirmed by the nonzero density of states at the Fermi level, and the presence of covalent bonds for all surface models is evidenced by a pseudogap near the Fermi level.

The PDOS from the third to innermost layers, except that of N(Ti)-terminated surface, is similar to that in bulk Ti_2AlN and other MAX phases in earlier reports [13,23]. The states near the Fermi level are dominated mainly by Ti-3d states. The strong (3d)Ti-(2p)N hybridization is located at the valence bands as expected for the covalent compound. The (3d)Ti-(3p)Al hybridization is located at a higher energy range than(3d)Ti-(2p)N hybridization, which is reasonable to conclude that the Ti-N bonds are relatively stronger than the Ti-Al bonds.

For N(Ti)-terminated surface in Fig. 7(a), the PDOS of outermost N and second Ti layers shifts to the high energy region, forming (3d)Ti-(2p)N hybridization in the range of − 5 eV to 0 eV. Accompanying the state shift of the second Ti layer, the (3p)Al in the third layer shifts towards the Fermi energy level to form (3d)Ti-(3p)Al hybridization. The PDOS redistribution from the outermost to third layers contributes to the structural reconstruction, Δd_{12} and Δd_{23}, in N(Ti)-terminated surface in Fig. 5(a) and (c). For Ti (N)-terminated surface in Fig. 7(b), the outermost Ti-3d state near the Fermi energy level is increased and the PDOS beyond the second layer is not changed compared with that in the inner layer, which is responsible for that structural relaxation only exists between first and second atomic layers in Fig. 5. For Al(Ti)- and Ti(Al)-terminated surfaces in Fig. 7(c) and (d), a similar PDOS redistribution emerges in the outermost and second atomic layers to form (3d)Ti-(3p)Al hybridization. It should be mentioned that the redistribution in outermost Ti layer of Ti(Al)-terminated surface is tremendous, wherein the states below −5 eV completely disappear and the state near the Fermi energy level is highly increased.

According to the calculated structural relaxation and surface energy at different temperatures, significant changes of the d-spacings of outermost Ti and N layers in N(Ti)- and Ti(N)-terminated surfaces happen between 933 K and 1273 K, and the metallic properties of Al(Ti)-terminated surface are different with that of Ti(Al)-terminated surface. The PDOS of dominant orbitals of outermost two layers at different temperatures are analyzed.

For N(Ti)- and Ti(N)-terminated surfaces, the bonding between outermost two layers mainly results from (3d)Ti-(2p)N hybridization. The calculated PDOS of N-2p and Ti-3d orbitals from 0 K to 1273 K are shown in Fig. 8. The Fermi energy level denoted by a black dashed line is set to zero. The pseudogap near the Fermi level is described by the two peaks with blue dashed lines. The N(Ti)-terminated surface exhibits nonmetallic property, while the Ti(N)-terminated surface shows metallic properties. The PDOS of dominant orbitals of outermost two layers keeps stable below 933 K. The states of hybridization between N-2p and Ti-3d are greatly changed at 1273 K compared with those below 933 K. The peak between −1 eV and −0.5 eV is gradually changed to be flatter for N(Ti)-terminated surface with increasing system temperature.

For Ti(N)-terminated surface, the PDOS peaks of both N-2p and Ti-3d shift to the high energy region with increasing temperature, and the PDOS peak of Ti-3d near the Fermi level shifts to high energy region till across the Fermi level between 933 K and 1273 K. As a result, the width of pseudogap of N(Ti)-terminated surface is widened from 1.61 eV at 933 K to 3.24 eV at 1273 K as well as 1.65 eV versus 4.70 eV for Ti(N)-terminated surface, which indicate that the Ti-N bonding is strengthened with increasing temperature between 933 K and 1273 K. The increased pseudogap width means enhanced hybridization to induce smaller outermost *d*-spacing with higher surface energy, which is responsible for the dramatical reduction of Δd_{12} and increase of surface energy from 933 K to 1273 K in Fig. 5(a) and 6. Furthermore, the strengthening Ti-N bonding with increasing temperature partially supports the experimental phenomenon of Ti_2AlN decomposing as TiN_x and aluminum steam at the temperature above 1673 K [5].

The calculated PDOS of Al-3p and Ti-3d orbitals from 0 K to 1273 K for Al(Ti)- and Ti(Al)-terminated surfaces are shown in Fig. 9. Compared with that of Al(Ti)-terminated surface, the PDOS of Ti(Al)-terminated surface shifts to high energy region with larger intensity near the Fermi level at all temperature, and the peaks below −4 eV completely disappear. The gathering states near the Fermi energy level mean the strengthening of metallic properties, which supports the result that the average CTE of d_{12} for Ti(Al)-terminated surface is much larger than that for Al(Ti)-terminated surface in Fig. 5(b). The states of electrons near the Fermi surface are usually used to identify the metallic properties of solid matter. With increasing temperature from 0 K to 1269 K, the states variations near the Fermi level show that the metallic properties of Al(Ti)- and Ti(Al)-terminated surfaces are gradually reduced.

4. Conclusions

In this study, the structural relaxation, surface energy and electronic property of $Ti_2AlN(0001)$ surfaces with different termination were studied by AIMD simulations at 0 K, 273 K, 600 K, 933 K and 1273 K. The main results are summarized as follows:

(1). Surface model with 7 atomic layers is thick enough to guarantee the inner bulk structure. The expansion of Ti_2AlN along [0001] direction with increasing temperature mainly results from the metallic bonds of Ti-Al layers.

(2). The structural relaxations of Ti(N)- and Ti(Al)-terminated surfaces are confined between the outermost two layers, and those of N(Ti)- and Al(Ti)-terminated surface extends among the outermost three layers. The results of surface energy show that Al(Ti)-terminated surface is the most stable surface at all temperature ranges.

(3). The structural shrinkage relaxation of outermost two layers at the ground state are sorted as N(Ti)-terminated > Ti(N)-terminated > Ti(Al)-terminated > Al(Ti)-terminated. For N(Ti)- and Ti(N)-terminated surfaces, the stable relaxation of outermost two layers dramatically increases from 933 K to 1273 K. While the relaxation of outermost two layers for Al(Ti)- and Ti(Al)-terminated surfaces changes with increasing system temperature. The metallic properties for Ti(Al)-terminated surface is stronger than that for Al(Ti)-terminated surface.

(4). The redistribution of Ti-3d orbitals of outermost or second layers is crucial to the electronic properties and structural relaxations of different termination surfaces. With increasing system temperature above 933 K, the pseudogap is highly widened for N(Ti)- and Ti(N)-terminated surfaces, corresponding to the strengthened Ti-N bonding and increased structural relaxation by enhanced (3d)

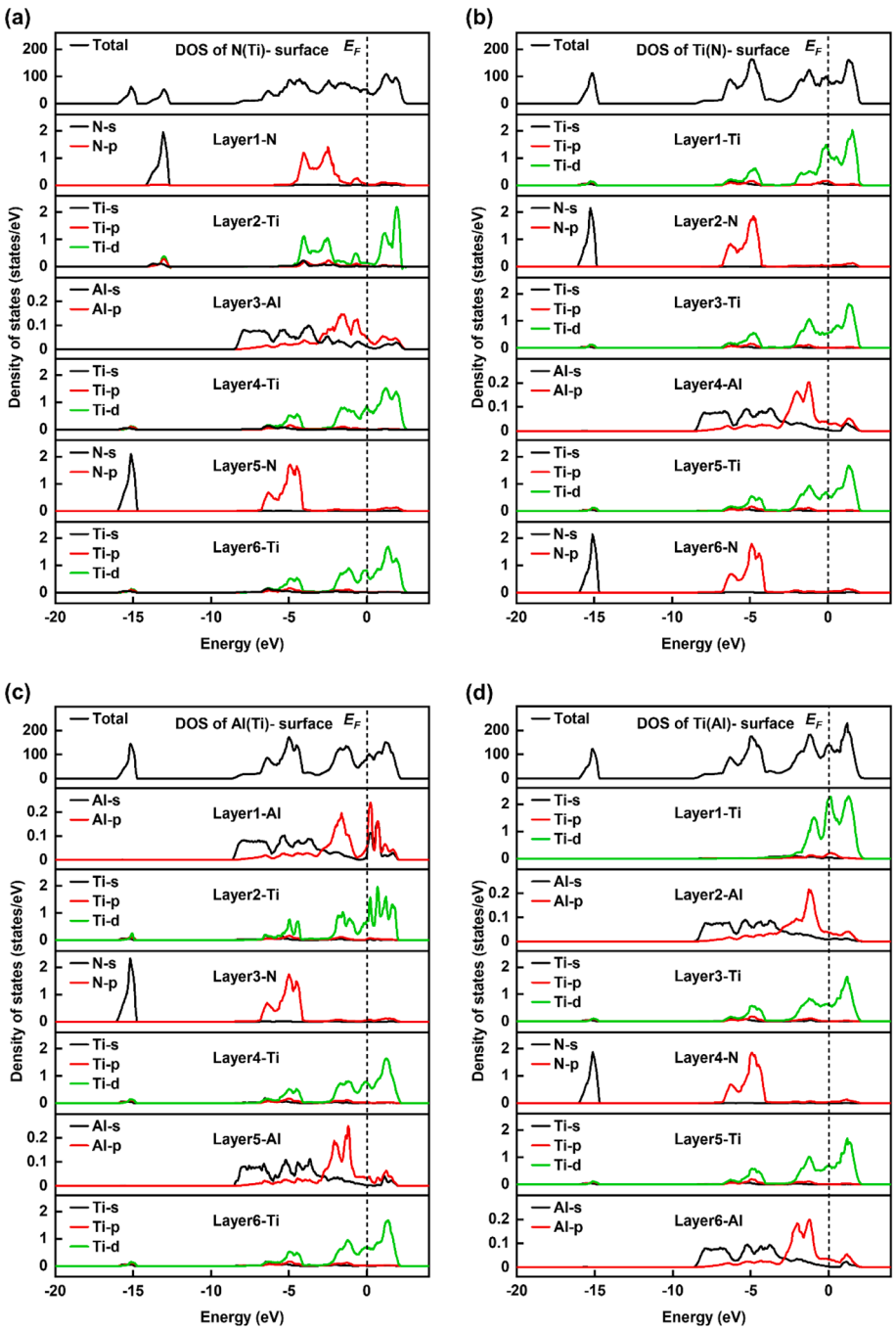

Fig. 7. Total DOS and layered PDOS of $Ti_2AlN(0001)$ surfaces at 0 K. (a) N(Ti)-terminated surface with 13 atomic layers; (b) Ti(N)-terminated surface with 15 atomic layers; (c) Al(Ti)-terminated surface with17 atomic layers; (d) Ti(Al)-terminated surface with 19 atomic layers.

Ti-(2p)N hybridization. With increasing temperature from 0 K to 1269 K, the metallic properties of Al(Ti)- and Ti(Al)-terminated surfaces are gradually reduced.

(5). The difference of structural shrinkage relaxation for N(Ti)-, Ti(N)-, Ti(Al)-and Al(Ti)-terminated surfaces, the strengthened Ti-N bonding and increased structural relaxation for N(Ti)- and Ti(N)-terminated surfaces between 933 K and 1273 K, and the stronger metallic property of Ti(Al)-terminated surface than that of Al(Ti)-terminated surface provide theoretical foundation for the termination selection and control of $Ti_2AlN(0001)$ surface in the application of heterogeneous nucleation and Al matrix composites.

CRediT authorship contribution statement

Biao Yu: Methodology, Investigation, Visualization, Writing – original draft. **Yanfeng Han:** Conceptualization, Methodology, Writing – review & editing, Supervision, Funding acquisition. **Dong Li:** Investigation, Resources. **Guangmin Hu:** Investigation, Resources. **Qing Dong:** Investigation, Resources. **Jiao Zhang:** Project administration. **Baode Sun:** Project administration.

Declaration of Competing Interest

The authors declare that they have no known competing financial interests or personal relationships that could have appeared to influence

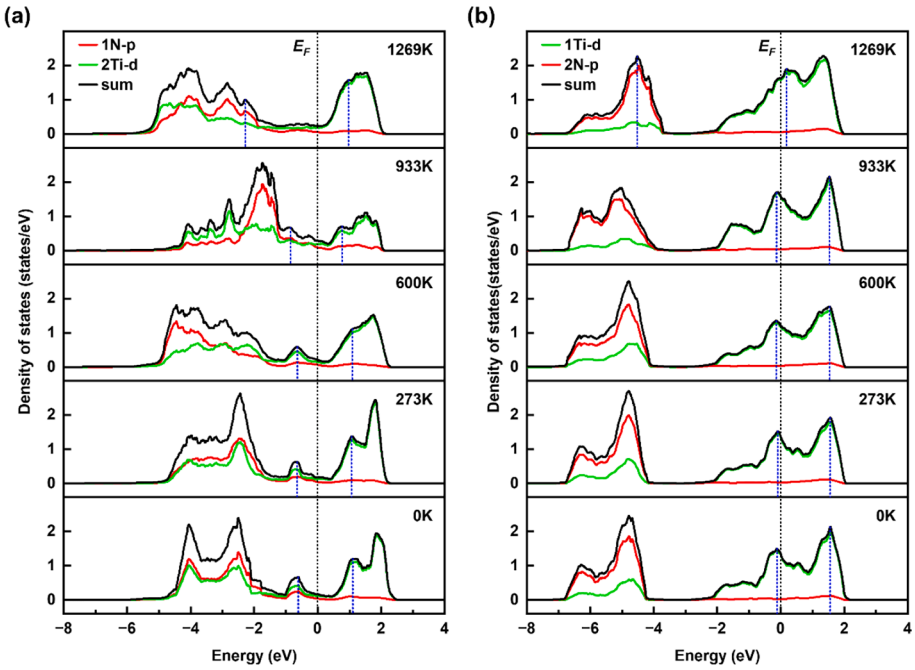

Fig. 8. PDOS of outermost and second layers for (a) N(Ti)-terminated surface with 13 layers and (b) Ti(N)-terminated surface with 15 layers at 0 K, 273 K, 600 K, 933 K and 1273 K.

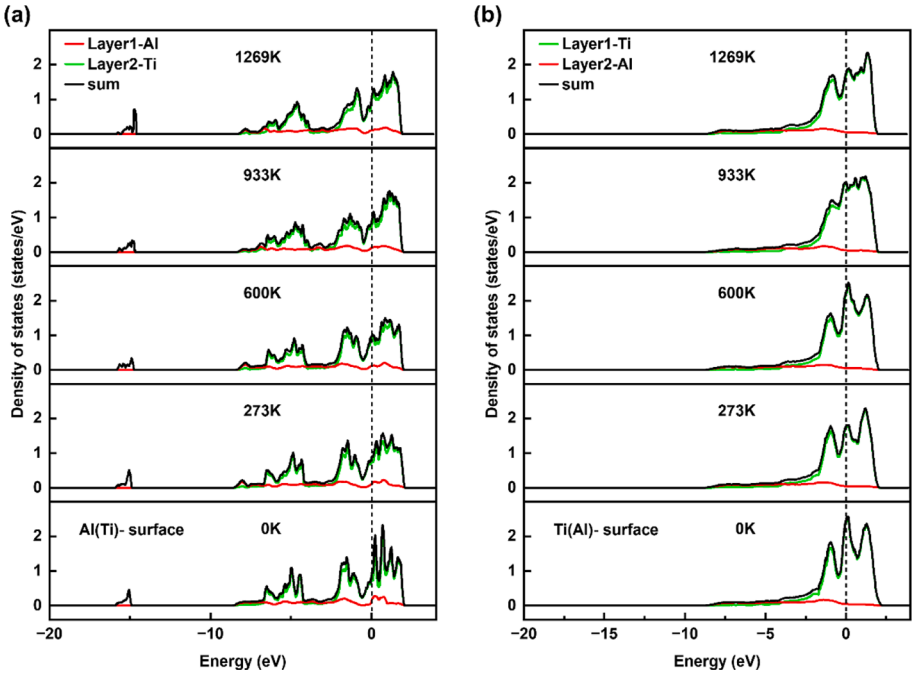

Fig. 9. PDOS of outermost and second layers at 0 K, 273 K, 600 K, 933 K and 1273 K. (a) Al(Ti)-terminated surface with 17 atomic layers; (b) Ti(Al)-terminated surface with 19 atomic layers.

the work reported in this paper.

Data availability

Data will be made available on request.

Acknowledgements

This work is financially supported by the National Key Research and Development Program of China (No. 2020YFB0311201) and National Natural Science Foundation of China (No. 52273230 and No. 51731007).

References

[1] T.C. Duong, N. Singh, R. Arróyave, First-principles calculations of finite-temperature elastic properties of Ti_2AlX (X=C or N), Computational Materials Science. 79 (2013) 296–302, https://doi.org/10.1016/j.commatsci.2013.06.033.
[2] M. Magnuson, M. Mattesini, S. Li, C. Höglund, M. Beckers, L. Hultman, O. Eriksson, Bonding mechanism in the nitrides Ti_2AlN and TiN: An experimental and

theoretical investigation, Physical Review B. 76 (2007) 195127, https://doi.org/10.1103/PhysRevB.76.195127.
[3] Z. Zhang, H. Jin, J. Chai, J. Pan, H.L. Seng, G.T.W. Goh, L.M. Wong, M.B. Sullivan, S.J. Wang, Temperature-dependent microstructural evolution of Ti_2AlN thin films deposited by reactive magnetron sputtering, Applied Surface Science. 368 (2016) 88–96, https://doi.org/10.1016/j.apsusc.2016.01.229.
[4] M. Chlewicka, A. Dobkowska, R. Sitek, B. Adamczyk-Cieślak, J. Mizera, Microstructure and corrosion resistance characteristics of Ti–AlN composite produced by selective laser melting, Materials and Corrosion. 73 (2022) 451–459, https://doi.org/10.1002/maco.202112703.
[5] I.M. Low, W.K. Pang, S.J. Kennedy, R.I. Smith, High-temperature thermal stability of Ti_2AlN and Ti_4AlN_3: A comparative diffraction study, Journal of the European Ceramic Society. 31 (2011) 159–166, https://doi.org/10.1016/j.jeurceramsoc.2010.09.014.
[6] B. Cui, R. Sa, D.D. Jayaseelan, F. Inam, M.J. Reece, W.E. Lee, Microstructural evolution during high-temperature oxidation of spark plasma sintered Ti_2AlN ceramics, Acta Materialia. 60 (2012) 1079–1092, https://doi.org/10.1016/j.actamat.2011.11.010.
[7] W. Liu, C. Qiu, J. Zhou, Z. Ding, X. Zhou, S. Du, Y.-H. Han, Q. Huang, Fabrication of Ti_2AlN ceramics with orientation growth behavior by the microwave sintering method, Journal of the European Ceramic Society. 35 (2015) 1385–1391, https://doi.org/10.1016/j.jeurceramsoc.2014.11.020.
[8] L. Gröner, L. Mengis, M. Galetz, L. Kirste, P. Daum, M. Wirth, F. Meyer, A. Fromm, B. Blug, F. Burmeister, Investigations of the deuterium permeability of as-deposited and oxidized ti_2aln coatings, Materials. 13 (2020) 2085, https://doi.org/10.3390/ma13092085.
[9] J. Feng, H. Xiao, Tribocorrosion behavior of laser cladded Ti-Al-(C, N) composite coatings in artificial seawater, Coatings. 12 (2022) 187, https://doi.org/10.3390/coatings12020187.
[10] Y. Liu, R. Hu, J. Yang, J. Li, Tensile properties and fracture behavior of in-situ synthesized Ti_2AlN/Ti48Al2Cr2Nb composites at room and elevated temperatures, Materials Science and Engineering: A. 679 (2017) 7–13, https://doi.org/10.1016/j.msea.2016.09.105.
[11] Y. Tan, H. Fang, Y. Liu, X. Wang, R. Chen, F. Cao, Y. Su, J. Guo, H. Fu, Regulating the macro/microstructure and mechanical properties of Ti_2AlN/Ti46Al4Nb1Mo composites via ultrasonic treatment, Materials Science and Engineering: A. 841 (2022) 143013, https://doi.org/10.1016/j.msea.2022.143013.
[12] J. Li, R. Hu, M. Zhou, Z. Gao, Y. Wu, X. Luo, High temperature micromechanical behavior of Ti_2AlN particle reinforced TiAl based composites investigated by in-situ high-energy X-ray diffraction, Materials & Design. 212 (2021) 110225, https://doi.org/10.1016/j.matdes.2021.110225.
[13] P. Liu, X. Han, D. Sun, Q. Wang, First-principles investigation on the structures, energies, electronic and defective properties of Ti_2AlN surfaces, Applied Surface Science. 433 (2018) 1056–1066, https://doi.org/10.1016/j.apsusc.2017.10.112.
[14] G. Jia, L. Yang, Ab initio calculations for properties of Ti_2AlN and Cr_2AlC, Physica B: Condensed Matter. 405 (2010) 4561–4564, https://doi.org/10.1016/j.physb.2010.08.038.
[15] J. Xiao, T. Yang, C. Wang, J. Xue, Y. Wang, Investigations on radiation tolerance of $M_{n+1}AX_n$ phases: Study of Ti_3SiC_2, Ti_3AlC_2, Cr_2AlC, Cr_2GeC, Ti_2AlC, and Ti_2AlN, Journal of the American Ceramic Society. 98 (2015) 1323–1331, https://doi.org/10.1111/jace.13450.
[16] N.J. Lane, S.C. Vogel, G. Hug, A. Togo, L. Chaput, L. Hultman, M.W. Barsoum, Neutron diffraction measurements and first-principles study of thermal motion of atoms in select $M_{n+1}AX_n$ and binary MX transition-metal carbide phases, Physical Review B. 86 (2012) 214301, https://doi.org/10.1103/PhysRevB.86.214301.
[17] A.V. Pshyk, E. Coy, M. Kempiński, B. Scheibe, S. Jurga, Low-temperature growth of epitaxial Ti_2AlC MAX phase thin films by low-rate layer-by-layer PVD, Materials Research Letters. 7 (2019) 244–250, https://doi.org/10.1080/21663831.2019.1594428.
[18] H. Högberg, P. Eklund, J. Emmerlich, J. Birch, L. Hultman, Epitaxial Ti_2GeC, Ti_3GeC_2, and Ti_4GeC_3 MAX-phase thin films grown by magnetron sputtering, Journal of Materials Research. 20 (2005) 779–782, https://doi.org/10.1557/JMR.2005.0105.
[19] X. Han, P. Liu, D. Sun, Q. Wang, Quantifying the role of interface atomic structure in the compressive response of Ti_2AlN/TiAl composite using MD simulations, Journal of Materials Science. 54 (2019) 5536–5550, https://doi.org/10.1007/s10853-018-03237-2.
[20] X. Han, P. Liu, D. Sun, Q. Wang, An atomic-level understanding of the friction and wear behaviors of Ti_2AlN/TiAl composite via MD simulations, Tribology International. 137 (2019) 340–348, https://doi.org/10.1016/j.triboint.2019.05.021.
[21] P. Liu, X. Han, D. Sun, Z. Chen, Q. Wang, Adhesion, stability and electronic properties of Ti_2AlN(0001)/TiAl(111) coherent interface from first-principles calculation, Intermetallics. 96 (2018) 49–57, https://doi.org/10.1016/j.intermet.2018.02.012.
[22] Phase stability of $Cr_{n+1}GaC_n$ MAX phases from first principles and Cr_2GaC thin-film synthesis using magnetron sputtering from elemental targets - Petruhins - 2013 - physica status solidi (RRL) – Rapid Research Letters - Wiley Online Library, (n.d.). https://onlinelibrary.wiley.com/doi/10.1002/pssr.201308025 (accessed February 15, 2023).
[23] M.W. Qureshi, X. Ma, X. Zhang, G. Tang, R. Paudel, D. Paudyal, Ab-initio predictions of phase stability, electronic structure, and optical properties of (0001)-MAX surfaces in M_2AC (M = Cr, Zr, Hf; A = Al, Ga), Journal of Physics and Chemistry of Solids. 160 (2022) 110338, https://doi.org/10.1016/j.jpcs.2021.110338.
[24] J. Ho, E. Heifets, B. Merinov, Ab initio simulation of the $BaZrO_3$ (001) surface structure, Surface Science. 601 (2007) 490–497, https://doi.org/10.1016/j.susc.2006.10.011.
[25] D. Music, Z. Sun, R. Ahuja, J.M. Schneider, Surface energy of M2AC(0001) determined by density functional theory (M=Ti, V, Cr; A=Al, Ga, Ge), Surface Science. 601 (2007) 896–899, https://doi.org/10.1016/j.susc.2006.11.025.
[26] G. Kresse, J. Furthmüller, Efficient iterative schemes for ab initio total-energy calculations using a plane-wave basis set, Physical Review B. 54 (1996) 11169–11186, https://doi.org/10.1103/PhysRevB.54.11169.
[27] G. Kresse, J. Furthmüller, Efficiency of ab-initio total energy calculations for metals and semiconductors using a plane-wave basis set, Computational Materials Science. 6 (1996) 15–50, https://doi.org/10.1016/0927-0256(96)00008-0.
[28] P.E. Blöchl, Projector augmented-wave method, Physical Review B. 50 (1994) 17953–17979, https://doi.org/10.1103/PhysRevB.50.17953.
[29] G. Kresse, D. Joubert, From ultrasoft pseudopotentials to the projector augmented-wave method, Physical Review B. 59 (1999) 1758–1775, https://doi.org/10.1103/PhysRevB.59.1758.
[30] J.P. Perdew, J.A. Chevary, S.H. Vosko, K.A. Jackson, M.R. Pederson, D.J. Singh, C. Fiolhais, Atoms, molecules, solids, and surfaces: Applications of the generalized gradient approximation for exchange and correlation, Physical Review B. 46 (1992) 6671–6687, https://doi.org/10.1103/PhysRevB.46.6671.
[31] B. Manoun, F.X. Zhang, S.K. Saxena, T. El-Raghy, M.W. Barsoum, X-ray high-pressure study of Ti_2AlN and Ti_2AlC, Journal of Physics and Chemistry of Solids. 67 (2006) 2091–2094, https://doi.org/10.1016/j.jpcs.2006.05.051.
[32] G. Hug, M. Jaouen, M.W. Barsoum, X-ray absorption spectroscopy, EELS, and full-potential augmented plane wave study of the electronic structure of Ti_2AlC, Ti_2AlN, Nb_2AlC, and $(Ti_{0.5}Nb_{0.5})_2AlC$, Physical Review B. 71 (2005) 024105, https://doi.org/10.1103/PhysRevB.71.024105.
[33] I.R. Shein, A.L. Ivanovskii, Graphene-like titanium carbides and nitrides $Ti_{n+1}C_n$, $Ti_{n+1}N_n$ (n=1, 2, and 3) from de-intercalated MAX phases: First-principles probing of their structural, electronic properties and relative stability, Computational Materials Science. 65 (2012) 104–114, https://doi.org/10.1016/j.commatsci.2012.07.011.